A General, One-Step and Template-Free Route to Rattle-Type Hollow Carbon Spheres and Their Application in Lithium Battery Anodes

ARTICLE *in* THE JOURNAL OF PHYSICAL CHEMISTRY C · JULY 2009

Impact Factor: 4.77 · DOI: 10.1021/jp901474w

A General, One-Step and Template-Free Route to Rattle-Type Hollow Carbon Spheres and Their Application in Lithium Battery Anodes

Rongbo Zheng,[†,§] Xianwei Meng,[†] Fangqiong Tang,[*,†] Lin Zhang,[†] and Jun Ren[†]

Laboratory of Controllable Preparation and Application of Nanomaterials, Technical Institute of Physics and Chemistry, Chinese Academy of Sciences (CAS), Beijing 100190, People's Republic of China, and Graduate School of CAS, Beijing 100039, People's Republic of China

Received: February 18, 2009; Revised Manuscript Received: May 28, 2009

A general, rapid, template-free, one-step, and continuous approach have been designed to rattle-type hollow carbon spheres (M@carbon, M = multiple Sn, Pt, Ag, or Fe-FeO nanoparticles) via ultrasonic spray pyrolysis of aqueous solutions containing sodium citrate and corresponding inorganic metal salts. The route involves the following three procedures: (1) initial generation of metal nanoparticles via the reduction of corresponding metal salts with sodium citrate in the hot liquid droplets and subsequent formation of a sodium citrate outer shell due to the tendency of free sodium citrate molecules to move to the periphery of the hot liquid droplets; (2) the formation of carbon outer shell via carbonization of the sodium citrate outer shell; and (3) the production of M@carbon via removing water-soluble byproduct. The content of encapsulated nanoparticles in M@carbon can be controlled via tuning the concentration of metal salts. Due to its novel structures, Sn@carbon exhibits high capacity and good cycle performance when they were used as anode materials for lithium batteries.

1. Introduction

Recently, rattle-type hollow spheres (i.e., hollow shells with a solid particle core and interstitial hollow space in between) have received attention due to their unique structures as well as potential applications in confined reaction vessels, the immobilization of biomolecules, catalysts, and lithium-ion batteries, etc.[1−8] Usually, rattle-type architectures can be denoted as core A@shell B, such as metal@silica,[2] metal@polymer,[3] metal@carbon,[4,5] oxide@carbon,[6] etc. To the A@B, the hollow spheres not only could act as a barrier to prevent encapsulated nanoparticles (NPs) from coalescencing,[5] but also could provide the unique interstitial void space to accommodate the huge volume variation of encapsulated NPs, which was important to improve cycle performance of lithium batteries.[4,9] As demonstrated by previous literatures,[4,9] Sn@carbon have exhibited higher capacity and better cycle performance as anode material in lithium batteries compared with pure Sn NPs. In addition, their inter void space could be utilized as scaffolds to encapsulate other NPs into hollow spheres,[7] and provide the catalytic reaction sites on the surface of encapsulated catalyst NPs.[5]

Inspired by these important characteristics, many research groups have devoted great effort to synthesize A@B. Besides some novel strategies,[4,10−12] two approaches to generate A@B were employed. One approach was the bottom-up approach, in which the core and shell were fabricated in an inside-to-outside order.[2−5,13−16] That is, the core NPs were first prepared, followed by consecutive coating with a spacer layer, and an outer layer made of targeted material. Finally, the spacer layer is removed via dissolution or calcination to produce A@B. For example, Xia's research group first exploited the bottom-up strategy to Au@polymer.[3] Aside from single NP, multiple NPs have been encapsulated via the bottom-up approach. Lou et al.[8] further extended the bottom-up route to prepare multiple Au NPs@silica via the following three steps: generation of Au NPs on the surface of amino-functionalized polystrene (PS) NPs, silica coating of PS@Au, and removal of PS via calcination. More recently, multiple tin NPs were encapsulated in hollow carbon spheres by Wan and co-workers via bottom-up strategy.[9] Alternatively, A@B could be generated via the top-down approach: the hollow spheres were first generated, followed by formation of the cores. For instance, $CoFe_2O_4$@carbon,[6,17] Cu@silica,[18] and Au@silica[19] have been successfully fabricated via the top-down strategy. Although various A@B have been produced,[2−19] most of the aforementioned approaches involved the templates and meantime employed multiple synthetic steps, which result in long reaction time and are inapplicable for continuous production on a large scale. For instance, the preparation of the template was generally tedious and postsynthetic treatments were usually needed to remove them from the products, which might destroy as-prepared hollow nanospheres.[7]

So, it is of interest to design a more convenient route to produce A@B to meet the requirements for practical application in fields such as confined reaction vessels, immobilization of biomolecules, catalysts, lithium-ion batteries, etc. In this paper, we report, for the first time, a general, one-step, rapid, template-free, and continuous approach to synthesize rattle-type hollow carbon spheres (M@carbon) via ultrasonic spray pyrolysis (USP)[20−23] of aqueous solutions containing sodium citrate and metal salts. Such a process is different from previous routes in many regards: (a) The initial reactant is low-cost and environmental friendly. Aqueous solutions containing sodium citrate and inorganic metal salts are used as precursors. (b) The route is general. Various functional NPs (e.g., Sn, Pt, Ag, or Fe-FeO) have been successfully encapsulated in hollow carbon spheres by selecting corresponding inorganic metal salts as the precursors. (c) The route is template-free. In the present paper, first, inner NPs are generated via reduction of metal salts with sodium citrate in the hot liquid droplets;[24,25] second, the sodium citrate outer shell is formed due to the tendency of free sodium citrate

* To whom correspondence should be addressed. E-mail: Tangfq@mail.ipc.ac.cn.
† Technical Institute of Physics and Chemistry, CAS.
§ Graduate School of CAS.

10.1021/jp901474w CCC: $40.75
Published on Web 07/07/2009

SCHEME 1: Illustration of the M@carbon Obtained via USP of Aqueous Solutions Containing Metal Salts and Sodium Citrate

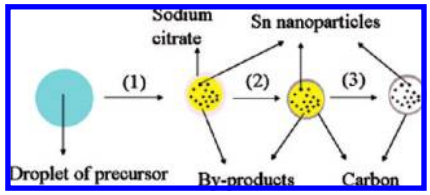

molecules to move to the periphery of the hot liquid droplets; third, a carbon outer shell is formed via carbonization of the sodium citrate shell; and finally, M@carbon is formed via removing water-soluble byproduct. (d) The route is rapid and continuous since an aerosol pyrolysis device is exploited.[20−23,26] (e) The content of encapsulated NPs in M@carbon can be tuned via changing the concentration of the metal salt. As an initial application, Sn@carbon exhibits high capacity and good cycle performance as the anode material for lithium-ion batteries.

2. Experimental Section

Sodium citrate, tin tetrachloride ($SnCl_4 \cdot 5H_2O$), ferrous chloride ($FeCl_2 \cdot 4H_2O$), hydrochloroplatinic acid ($H_2PtCl_6 \cdot 6H_2O$), and silver nitrate ($AgNO_3$) were obtained from Beijing Chemical Reagent Company. All chemicals were of analytic grade and were used without further purification.

The USP experimental setup was similar to that of Suslick's group.[20−23] In a typical experiment, sodium citrate (2.0 g) and $SnCl_4$ (0.6 g) were added to deioned water (100 mL) so as to form a precursor solution. For nebulization, a Yuyue ultrasonic nebulizer was used to nebulize precursor aqueous solution into fine mist droplets. The furnace temperature was set as 700 °C with a nitrogen flow rate of 2 SLPM (Standard Liters per Minute). After being washed with deioned water and then ethanol three more times, Sn@carbon was collected for further analysis. Similarly, Pt@carbon, Ag@carbon, and Fe-FeO@carbon could be fabricated via simply replacing $SnCl_4$ with H_2PtCl_6 (0.6 mL, 0.02 g/mL), $AgNO_3$ (0.1 g), and $FeCl_2$ (0.15 g), respectively.

Test cells were assembled in an Ar-filled glovebox (MBraun, Lab Master 130) for evaluating the electrochemical performances of Sn@carbon. The working electrode was prepared by casting a mixture of the Sn@carbon (90 wt %), polyvinylidene fluoride (PVDF, 5 wt %) dissolved in *N*-methylpyrrolidone (NMP), and carbon black (5 wt %) on a copper foil. The aforementioned foil was then dried under vacuum at 100 °C for 8 h. Lithium−metal foil was used as the counter electrode, $LiPF_6$ (1 M) dissolved in a mixture of ethylene carbonate (EC) and dimethyl carbonate (DMC) (1:1 in volume) was used as the electrolyte, and Celgard 2400 was used as the separator. The cell was galvanostatically cycled between 0.0 and 3.0 V (vs Li) at a current density of 0.55 mA/cm^2.

X-ray diffraction (XRD) patterns were obtained on Rigaku Dmax2000 with Cu Kα radiation. The morphology of the samples was examined by scanning (SEM, XL30ESEM FEG) and transmission (TEM, JEOL 2010) electron microscopy thermogravimetrics (TG, Perkin-Elmer thermal analysis equipment).

3. Results and Discussion

Scheme 1 illustrates the formation mechanism of M@carbon. In the present approach, aerosol liquid droplets are produced via ultrasonic spray treatment of precursor aqueous solutions.

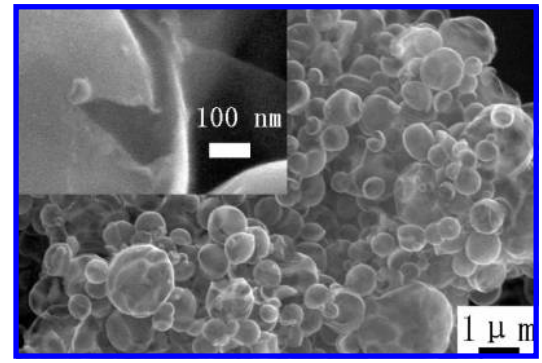

Figure 1. SEM images of carbon hollow spheres obtained via USP of single sodium citrate aqueous solutions. The inset is the magnified SEM images.

In the case of a quartz-glass tube in a hot furnace, the temperature is lower (near room temperature) at the two ends, while the temperature is highest (e.g., 700 °C) in the center of the quartz-glass tube. Then, as the liquid droplets are carried in the nitrogen stream through a quartz-glass tube in a hot furnace, the temperature of the above liquid droplets will be increased from near room temperature to the boiling state. That is, there is a transition stage where droplets exist as hot liquid before changing to the solid state via evaporation of water. On the other hand, Dong et al. have demonstrated that a higher concentration of sodium citrate could reduce $HAuCl_4$ to form gold nanoparticles even at room temperature.[27] Thus, we proposed that Sn, Pt, Ag, or Fe nanoparticles are generated via reducing the reaction between a high concentration of sodium citrate and the corresponding metal salts in the hot liquid droplets.

The formation mechanism can be presented as follows. First, as the liquid droplets are carried in the nitrogen stream through a quartz-glass tube in a hot furnace, the temperature of the above liquid droplets increases, which leads to the reduction of the metal ion (such as Sn^{4+}, $PtCl_6^{2-}$, Ag^+, or Fe^{2+}, etc.) with sodium citrate to form the corresponding metal NPs.[24,25] In comparison with the aforementioned NPs, the size of the free sodium citrate molecules is smaller. With the evaporation of the water, smaller particles (i.e., free sodium citrate molecules) move more rapidly to the periphery of the hot liquid droplets to form a sodium citrate outer shell due to capillary force in the liquid droplet, which is similar to the formation procedure of microencapsulated larger-NPs/smaller-NPs powders via aerosol spray of aqueous solutions containing two types of NPs of different size.[28] Second, with the temperature further increased, the sodium citrate outer shell will carbonize to form a carbon outer shell. As shown in Figure 1, the hollow carbon spheres with a size of about 1 μm are obtained via USP of sodium citrate aqueous solution, which further indicates that the carbon outer shell is generated via carbonization of the sodium citrate outer shell. Finally, M@carbon (M = Sn, Pt, Ag, or Fe-FeO nanoparticles) is generated via removing water-soluble byproduct (such as NaCl, Na_2CO_3, etc.) in water.

As a typical example, using aqueous solutions containing $SnCl_4$ and sodium citrate as precursors, Sn@carbon can be produced via USP. Figure 2 is the XRD pattern of the corresponding sample obtained. The diffraction peaks in Figure 2A can be easily indexed as tetragonal-structured Sn (JCPDS 04-0673). No obvious impurity phases, such as SnO and SnO_2, can be detected in Figure 2A. The morphology of the synthesized Sn@carbon is examined by using SEM and TEM. As shown in Figure 3A, the sample consists of microspheres with

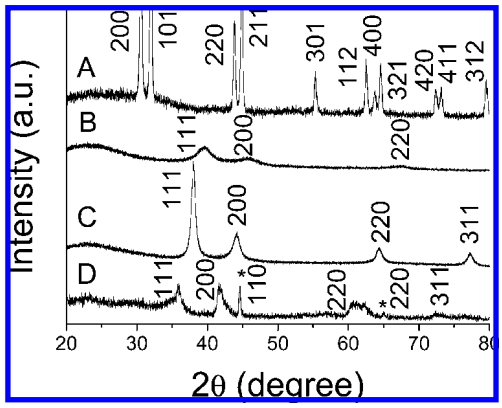

Figure 2. XRD patterns of (A) Sn@carbon, (B) Pt@carbon, (C) Ag@carbon, and (D) Fe-FeO@carbon obtained via USP of aqueous solutions containing sodium citrate and corresponding metal salts. The peaks with an asterisk in D can be indexed to metallic Fe (JCPDS 85-1410).

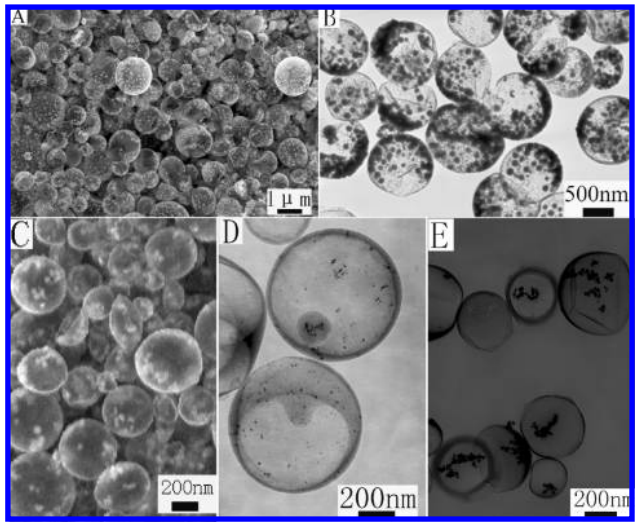

Figure 3. SEM and TEM images of (A and B) Sn@carbon, (C) Fe-FeO@carbon, (D) Pt@carbon, and (E) Ag@carbon obtained via USP of aqueous solutions containing sodium citrate and the corresponding metal salts.

a size range of 0.5−1.5 μm. Some concaved spheres reveal their hollow interior structures. Multiple NPs with a size of less than 100 nm are encapsulated in the interior of the hollow microspheres, which can be revealed by the smooth surface of hollow spheres. The TEM image (Figure 3B) further demonstrates that these NPs are studded onto the inner surface of the hollow spheres. The shell thickness of the hollow carbon sphere is about 20 nm. In comparison with the shell, these NPs appear as brighter spots in the SEM image and as darker spots in the TEM image, which further demonstrate the formation of metallic tin.

Thermogravimetric analysis (TGA) is performed to obtain the content of Sn in Sn@carbon. As shown in Figure S1 in the Supporting Information, before 286 °C, the mass decreases gradually with the temperature increase due to the loss of water, while there is a phenomenon of increase in mass between 286 and 315 °C, which can be ascribed to the oxidization of metallic Sn to form SnO_2 under higher temperature in air.[9] The mass rapidly decreases when the temperature increases to about 315 °C owing to the oxidization of carbon to generate CO_2 gas. The mass remains constant at 58.3% when the temperature reaches above 448 °C, which means only SnO_2 remained. The Sn content in the Sn@carbon is 46 wt %, which is measured from the TGA (Figure S1, Supporting Informatiuon).[9]

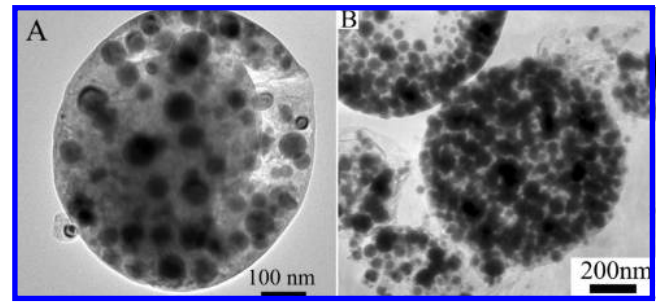

Figure 4. TEM images of Sn@carbon solids (A) collected without water at 700 °C and (B) collected with water at 500 °C.

To investigate the formation mechanism of Sn@carbon, the following control experiments are performed. As shown in Figure 4A, the TEM image of solids collected without water shows that the morphology is semisolid spheres instead of rattle-type hollow spheres. The results of XRD (Figure S2, Supporting Informatiuon) and EDS (Figure S3, Supporting Informatiuon) further reveal that there are water-soluble byproducts, such as NaCl and Na_2CO_3, etc. As revealed by the results of Suslick et al., carbon and water-soluble byproducts (e.g., NaCl, Na_2CO_3, polyaromatic hydrocarbons, etc.) have been generated via USP of aqueous solutions containing substituted alkali carboxylates or substituted alkali benzoates.[22,23] Thus, the byproduct in our procedure will contain NaCl, Na_2CO_3, and polyaromatic hydrocarbons, etc., since sodium citrate (a kind of alkali carboxylate) is used as the carbon source. When the reaction temperature decreases from 700 to 500 °C, using aqueous solutions containing sodium citrate and $SnCl_4$ as precursors, Sn NPs (Figure S4, Supporting Informatiuon) spherical aggregation with a thinner carbon shell is formed (Figure 4B). USP at 500 °C of sodium citrate aqueous solutions produces no carbonaceous solids although a slight discoloration is observed. Furthermore, the Au@carbon (data not shown) would be generated via USP of aqueous solutions containing citrate-stabilized Au NPs[24] and sodium citrate, which further demonstrated the above formation mechanism.

Similarly, noble metal (e.g., Pt and Ag) and magnetic (e.g., Fe-FeO) NPs can be encapsulated in hollow carbon spheres to form Pt@carbon, Ag@carbon, or Fe-FeO@carbon via simply replacing $SnCl_4$ with the corresponding inorganic metal salts. As indicated in Figure 2B, all the diffraction peaks can be indexed to cubic face-centered Pt (JCPDS 04-0802) if H_2PtCl_6 is exploited as metal salts. Cubic face-centered Ag (JCPDS 04-0783) can be generated when $AgNO_3$ is used as metal salts (Figure 2C). Different from Pt and Sn, the mixed phases of Fe (JCPDS 85-1410) and FeO (JCPDS 77-2355) are formed when $FeCl_2$ is used as metal salts. Multiple Fe-FeO NPs with a size of about 100 nm are also encapsulated in single hollow carbon spheres (Figure 3C). As shown in Figure 3D, multiple Pt NPs with a size of about 10 nm are encapsulated in hollow carbon spheres. When $AgNO_3$ is used as metal salts, Ag NPs with a size of about 30 nm are encapsulated in hollow carbon spheres (Figure 3E).

Moreover, the content of encapsulated NPs in M@carbon can be controlled via the variation of metal salt concentration because the formation of hollow carbon spheres is independent of the existence of metal salt (Figure 1). As shown in Figure 5, the number of Sn NPs in a single carbon hollow sphere decreases when the amount of $SnCl_4$ decreases to 0.12 g with the other conditions remaining constant. The result of EDX further demonstrates that the Sn content in Sn@carbon is about 6 wt %. The content of Sn increases to about 62 wt % when

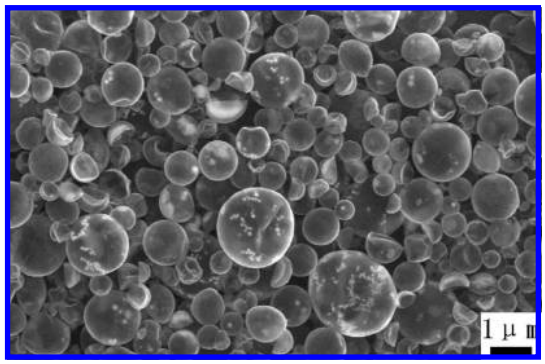

Figure 5. SEM images of Sn@carbon obtained with a fifth the concentration of $SnCl_4$ in Figure 2A.

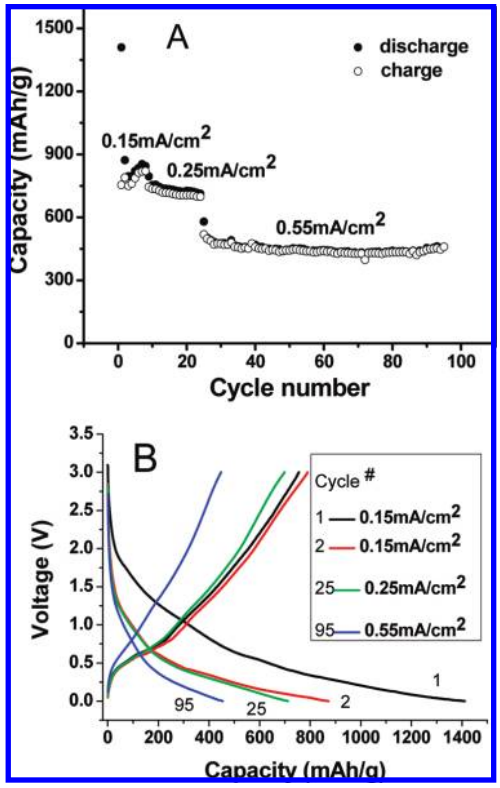

Figure 6. (A) The cycling performance in the 0 mV−3 V (vs. Li^+/Li) voltage window and (B) voltage profiles at different rate of Sn@carbon (46 wt % Sn).

the amount of $SnCl_4$ increases to 1.2 g with the other conditions remaining constant. As shown in Figure S5 in the Supporting Information, it is hard to obtain intact spherical morphology as sodium citrate almost reacts with $SnCl_4$, which further demonstrated the formation mechanism of M@carbon.

Because of the rapid development of lithium-ion batteries, it is very necessary to explore the electrochemical performance of our Sn@carbon as anode materials for lithium batteries on account of their particular structure.[4,9] Figure 6A shows the cycling performance of Sn@carbon (46 wt % Sn) as an anode in a cell with lithium metal as the counter electrode and a $LiPF_6$−ethylene carbonate−dimethylcarbonate solution as the electrolyte. The cell was galvanostatically cycled between 0.0 and 3.0 V (vs. Li). As demonstrated by previous literature, pure metallic Sn NPs tended to aggregate to be larger particles, and eventually pulverized to lose its Li^+ storage ability during the first several charge−discharge cycles.[4,20,30] The present Sn@carbon as anode materials for lithium batteries have a specific capacity higher than 460 mA h g^{-1} after the 95th cycle (Figure 6). It should be noted that, although our Sn@carbon anode exhibits a Coulombic efficiency of 53% in the first cycle, more than 90% is from the second cycle. TEM images of the Sn@carbon anode after the 10th cycle (Figure S6, Supporting Information) show that some inner Sn NPs have aggregated, but the aggregation of tin NPs inside a single carbon shell cannot ruin the carbon shell since there is enough void space to compensate for the volume expansion during the Li-insertion process. That is, the Sn@carbon anode does not pulverize during the cycle process due to the protection of carbon shells. From Figure S6 in the Supporting Information, we can see that some Sn nanoparticles do not electrochemically react with lithium to form alloys even after the 10th cycle. In the next cycle, the aforementioned Sn nanoparticles might react with lithium to form alloys, which may lead to the slight increase in capacity with cycling at the 0.15 mA/cm^2 rate. Considering the particular structure of Sn@carbon, four important factors should be responsible for the above excellent electrochemical performance. First, the hollow carbon sphere acts as a barrier to prevent the aggregation of tin NPs in different Sn@carbon. Second, the hollow carbon provides a void space to accommodate the huge volume variations, which ensures the good cycle characteristics. Third, multiple smaller Sn particles (about 100 nm) are encapsulated in a single carbon hollow sphere, thus resulting in smaller Sn NPs at the relatively high content of tin.[4,9] Fourth, the carbon shell is thin (about 20 nm), which provides very high weight capacity.

4. Conclusions

In summary, we have designed a general, one-step, rapid, template-free, and continuous approach to synthesize M@carbon via USP of aqueous solutions containing sodium citrate and metal salts. Rattle-type hollow carbon spheres, such as Sn@carbon, Pt@carbon, Ag@carbon, and Fe-FeO@carbon, have been successfully synthesized via select corresponding metal salts as the precursors. Since the formation of hollow carbon spheres is independent of the presence of metal salt, the content of encapsulated NPs (e.g., Sn) could be tuned via simply changing the initial concentration of metal salts. Thanks to their novel structures, Sn@carbon exhibits high capacity and good cycle performance (~460 mA h g^{-1} after the 95th cycle) when they were used as anode materials for lithium batteries. Finally, this convenient route can probably be extended to encapsulate other functional cores, such as Au, Pd, NiO, etc., in hollow carbon spheres.

Acknowledgment. Financial support for this research was provided by the Hi-Tech Research and Development Program of China (863) (2006AA03Z302, 2009AA03Z322) and the National Natural Science Foundation of China (60736001). We thank Dr. Bingkun Guo for the help with the Li-ion battery and the reviewers for their helpful comments.

Supporting Information Available: SEM images of M@carbon with different Sn content, SEM, XRD, EDS of Sn@carbon solid collected without water, TEM image of Sn@carbon anode after the 10th cycle, and the TG of Sn@carbon. This material is available free of charge via the Internet at http://pubs.acs.org.

References and Notes

(1) Lou, X. W.; Archer, L. A.; Yang, Z. C. *Adv. Mater.* **2008**, *20*, 3987.
(2) Kim, M.; Sohn, K.; Na, H. B.; Hyeon, T. *Nano Lett.* **2002**, *2*, 1383.
(3) Kamata, K.; Lu, Y.; Xia, Y. N. *J. Am. Chem. Soc.* **2003**, *125*, 2384.

(4) Lee, K. T.; Jung, Y. S.; Oh, S. M. *J. Am. Chem. Soc.* **2003**, *125*, 5652.
(5) Ikeda, S.; Ishino, S.; Harada, T.; Okamoto, N.; Sakata, T.; Mori, H.; Kuwabata, S.; Torimoto, T.; Matsumura, M. *Angew. Chem., Int. Ed.* **2006**, *45*, 7063.
(6) Fuertes, A. B.; Sevilla, M.; Valdés-Solís, T.; Tartaj, P. *Chem. Mater.* **2007**, *19*, 5418.
(7) Choi, W. S.; Koo, H. Y.; Kim, D. Y. *Langmuir* **2008**, *24*, 4633.
(8) Lou, X. W.; Yuan, C. L.; Rhoades, E.; Zhang, Q.; Archer, L. A. *Adv. Funct. Mater.* **2006**, *16*, 1679.
(9) Zhang, W. M.; Hu, J. S.; Guo, Y. G.; Zheng, S. F.; Zhong, L. S.; Song, W. G.; Wan, L. J. *Adv. Mater.* **2008**, *20*, 1160.
(10) Chen, H. Y.; Zhao, Y.; Song, Y. L.; Jiang, L. *J. Am. Chem. Soc.* **2008**, *130*, 7800.
(11) Ng, Y. H.; Ikeda, S.; Harada, T.; Higashida, S.; Sakata, T.; Mori, H.; Matsumura, M. *Adv. Mater.* **2007**, *19*, 597.
(12) Lou, X. W.; Yuan, C. L.; Zhang, Q.; Archer, L. A. *Angew. Chem., Int. Ed.* **2006**, *45*, 3825.
(13) Zhang, K.; Zhang, X. H.; Chen, H. T.; Chen, X.; Zheng, L. L.; Zhang, J. H.; Yang, B. *Langmuir* **2004**, *20*, 11312.
(14) Liu, S. H.; Zhang, Z. H.; Han, M. Y. *Adv. Mater.* **2005**, *17*, 1862.
(15) Arnal, P. M.; Comotti, M.; Schüth, F. *Angew. Chem., Int. Ed.* **2006**, *45*, 8224.
(16) Zhao, W. R.; Chen, H. R.; Li, Y. S.; Li, L.; Lang, M. D.; Shi, J. L. *Adv. Funct. Mater.* **2008**, *18*, 2780.
(17) Valdés-Solís, T.; Valle-Vigón, P.; Sevilla, M.; Fuertes, A. B. *J. Catal.* **2007**, *251*, 239.
(18) Hah, H. J.; Um, J. I.; Han, S. H.; Koo, S. M. *Chem. Commun.* **2004**, 1012.
(19) Cavaliere-Jaricot, S.; Darbandi, M.; Nann, T. *Chem. Commun.* **2007**, 2031.
(20) Skrabalak, S. E.; Suslick, K. S. *J. Am. Chem. Soc.* **2005**, *127*, 9990.
(21) Suh, W. H.; Jang, A. R.; Suh, Y. H.; Suslick, K. S. *Adv. Mater.* **2006**, *18*, 1832.
(22) Skrabalak, S. E.; Suslick, K. S. *J. Am. Chem. Soc.* **2006**, *128*, 12642.
(23) Skrabalak, S. E.; Suslick, K. S. *J. Phys. Chem. C* **2007**, *111*, 17807.
(24) Frens, G. *Nature (London), Phys. Sci.* **1973**, *241*, 20.
(25) Guo, S. J.; Wang, L.; Dong, S. J.; Wang, E. K. *J. Phys. Chem. C* **2008**, *112*, 13510.
(26) Tartaj, P.; González-Carreño, T.; Serna, C. J. *Adv. Mater.* **2001**, *13*, 1620.
(27) Wang, T.; Zheng, R. B.; Hu, X. G.; Zhang, L. X.; Dong, S. J. *J. Phys. Chem. B* **2006**, *110*, 14179.
(28) Iskandar, F.; Chang, H.; Okurama, K. *Adv. Powder Technol.* **2003**, *14*, 349.
(29) Courtney, I. A.; McKinnon, W. R.; Dahn, J. R. *J. Electrochem. Soc.* **1999**, *146*, 59.
(30) Li, H.; Shi, L.; Lu, W.; Huang, X.; Chen, L. *J. Electrochem. Soc.* **2001**, *148*, A915.

JP901474W